Combustion Theory and Modelling
Vol. 15, No. 4, 2011, 437–454

Strained premixed flames: Effect of heat-loss, preferential diffusion and reversibility of the reaction

Joel Daou*

University of Manchester, School of Mathematics, Manchester, M60 1QD, UK

(*Received 29 June 2010; final version received 19 November 2010*)

We provide an analytical description of the effect of preferential diffusion and volumetric heat-loss on strained premixed flames within a *reversible* chemistry model. The model comprises a single reversible reaction of the form $F \rightleftharpoons P$ whose forward and backward rates follow an Arrhenius law. An asymptotic analysis of the problem is carried out in the limit of infinitely large activation energy of the forward reaction. The study allows for non-unit Lewis numbers for the fuel F and the product P. Two main contributions are made.

The first contribution consists in identifying the fundamental differences in the asymptotic description of the *non-adiabatic* flame between the reversible and irreversible cases, and resolving the difficulties by a suitable generalization of the so-called near-equidiffusion flame approximation to the reversible case, including the derivation of appropriate jump conditions at the reaction sheet. This is used to demonstrate that the one-step reversible chemistry model is reducible to the classical irreversible chemistry model, provided that an effective reduced Lewis number $\bar{l}$ and an effective heat-loss parameter $\bar{\kappa}$ are used.

The second contribution is the determination of the domain of the solutions and their multiplicity, for selected values of $\bar{l}$, in the $\bar{\kappa}$-ϵ plane, where ϵ is a non-dimensional measure of the strain rate. For $\bar{l} < 4.03$, the diagrams are found to consist of four regions with one, two, three, and four solutions respectively, including the frozen solution. For $4.03 < \bar{l} < 5.15$, an additional region with three solutions is identified. For larger values of $\bar{l}$, the two regions with three solutions merge, and the region with four solutions is of insignificant size. Our diagrams are found to be in good agreement with, and complementary to, numerically determined diagrams in flammability limit studies based on one-step and detailed chemistry models. They are also a valuable component in studying non-adiabatic premixed edge-flames.

Keywords: premixed flames; reversible reaction; large activation energy asymptotics; flammability limits; non-adiabatic flames; edge-flames

1. Introduction

Over the last few decades, the counterflow configuration has been extensively adopted in theoretical, experimental and numerical studies, as a means to investigate various physical effects on real flames, such as stretch, preferential diffusion, radiation and chemical kinetics. Examples that are relevant to this work include studies on one-dimensional twin-flames, a problem of high significance to the determination of flammability limits [1–5], and investigations of two-dimensional premixed edge-flames in this configuration [6–9]. In this

*E-mail: joel.daou@manchester.ac.uk

ISSN: 1364-7830 print / 1741-3559 online

DOI: 10.1080/13647830.2010.545896
http://www.informaworld.com

latter context, the determination of the existence and multiplicity of the one-dimensional solutions is fundamental since they are the boundary conditions for the two-dimensional solutions far downstream and far upstream. In fact, this context provides a strong motivation for this work, especially with regard to the effect of preferential diffusion on the existence and multiplicity of the one-dimensional solutions in a strain-rate versus heat-loss-intensity plane. This aspect has been only partially and indirectly addressed in available numerical studies that are mainly concerned with flammability limits [2–5]. These studies have been based both on single-step and detailed chemistry models, and suggest that the predictions of the classical one-step irreversible model are quite robust, at least qualitatively. We shall test this robustness analytically, by considering a reversible chemistry model.

In fact, the reversibility of the reaction is a fundamental realistic aspect which does not seem to have been considered in the premixed counterflow configuration, at least in analytical investigations. This aspect is known to be a significant factor in combustion phenomena, such as the burning of hydrocarbons or high-caloric fuels in oxygen, if, for example, realistic values of the flame temperature are to be obtained, see [10, p. 25]. This significance of reversibility has been recognized in both unpremixed combustion [11, 12], and premixed combustion [13–16]. In the available analytical studies however, account of reversibility for flames subject to heat-loss does not seem to have been addressed. In fact, the theoretical (asymptotic) analysis of non-adiabatic flames with even the simplest reversible chemistry model presents non-trivial and interesting problems. As we shall show in this paper, there are fundamental differences in the asymptotic description of the non-adiabatic flame between the reversible and irreversible cases, with the main difficulty identified being that the reaction rate in the burnt gas is not transcendentally small in the former case.

Thus, one of our objectives is to present the first analytical study of flames incorporating reversibility and volumetric heat-loss, and to identify and resolve the corresponding difficulties. A second objective is to provide an analytical description of planar non-adiabatic strained flames, complementing the results of [1]. In particular, we wish to describe the influence of preferential diffusion on the existence and multiplicity of the non-adiabatic planar solutions in the various regions of strain-rate versus effective heat-loss diagrams. The findings may be useful in studies concerned with flammability limits, premixed edge-flames, turbulent combustion flamelet modelling, among others.

The paper is structured as follows. We first formulate the one-dimensional problem including a reversible reaction in the counterflow configuration, using the thermodiffusive (constant density) approximation for sake of simplicity and tractability. This is followed by an asymptotic analysis which leads to a full analytical description. The results, including generic bifurcation diagrams and useful formulas, are then presented and discussed with reference to related investigations in the literature which are mostly concerned with flammability limits. A summary of the main contributions concludes the paper.

2. Formulation

Figure 1 illustrates the configuration under consideration, including the planar twin-flames. Constant density is assumed throughout and the counterflow velocity is given by $\mathbf{v} = (ax, -ay)$, where a is the (dimensional) strain rate. To capture the effect of the reversibility of the chemistry in the simplest way, a single reversible reaction is assumed to take place in a fuel-lean mixture and to be of the form

$$\mathrm{F} \rightleftharpoons \mathrm{P} + q,$$

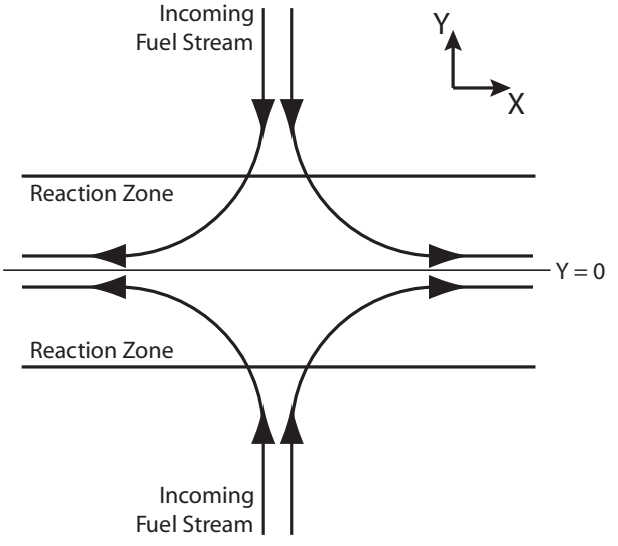

Figure 1. The counterflow configuration and the twin planar premixed flames.

where F, P and q represent the fuel, the product and the heat of reaction. The overall reaction rate $\hat{\omega}$ is taken to follow an Arrhenius law in the forward and backward directions of the form

$$\hat{\omega} = \rho Y_F B e^{-E/RT} - \rho Y_P B' e^{-E'/RT}.$$

Here ρ, Y_F, Y_P, R, T, B, E, B', and E' are the density, fuel mass fraction, product mass fraction, the universal gas constant, the temperature, the pre-exponential factor and the activation energy of the forward reaction and the pre-exponential factor and the activation energy of the backward reaction, respectively.

The one-dimensional governing equations are

$$-aY\frac{dT}{dY} = D_T\frac{d^2T}{dY^2} + \frac{q}{c_p}\frac{\hat{\omega}}{\rho} - \hat{\kappa}(T - T_u) \tag{1}$$

$$-aY\frac{dY_F}{dY} = D_F\frac{d^2Y_F}{dY^2} - \frac{\hat{\omega}}{\rho} \tag{2}$$

$$-aY\frac{dY_P}{dY} = D_P\frac{d^2Y_P}{dY^2} + \frac{\hat{\omega}}{\rho}, \tag{3}$$

where D_T, D_F and D_P represent the diffusion coefficients for heat, for the fuel and for the product, respectively. The term $\hat{\kappa}(T - T_u)$ in Equation (1), where T_u is the temperature of the incoming fuel streams, is intended to account for heat-loss in a simple way.

Given the symmetry of the configuration about the plane $Y = 0$, we need only solve the problem for $Y > 0$ with the boundary conditions

$$T = T_u\,,\ Y_F = Y_{F,u}\,,\ Y_P = 0 \quad \text{as } Y \to \infty$$

$$\frac{dT}{dY} = \frac{dY_F}{dY} = \frac{dY_P}{dY} = 0 \qquad \text{at } Y = 0\,.$$

The equations can be written in non-dimensional form as

$$-2y\frac{d\theta}{dy} = \frac{d^2\theta}{dy^2} + \epsilon^{-2}\omega - \epsilon^{-2}\frac{\kappa\theta}{\beta} \tag{4}$$

$$-2y\frac{dy_F}{dy} = \frac{1}{\mathrm{Le_F}}\frac{d^2y_F}{dy^2} - \epsilon^{-2}\omega \tag{5}$$

$$-2y\frac{dy_P}{dy} = \frac{1}{\mathrm{Le_P}}\frac{d^2y_P}{dy^2} + \epsilon^{-2}\omega, \tag{6}$$

with the boundary conditions

$$\theta = 0,\ y_F = 1,\ y_P = 0 \quad \text{as } y \to +\infty \tag{7}$$

$$\frac{d\theta}{dy} = \frac{dy_F}{dy} = \frac{dy_P}{dy} = 0 \quad \text{at } y = 0\,. \tag{8}$$

Here $\mathrm{Le_F} \equiv D_T/D_F$ and $\mathrm{Le_P} \equiv D_T/D_P$ are the Lewis numbers of the fuel and product, respectively. We have also used the Zeldovich number (the non-dimensional activation energy of the forward reaction) $\beta \equiv E(T_e - T_u)/RT_e^2$ and the scaled variables θ, y_F and y_P defined by

$$\theta = \frac{T - T_u}{T_e - T_u},\ y_F = \frac{Y_F - Y_{Fe}}{Y_{Fu} - Y_{Fe}},\ y_P = \frac{Y_P}{Y_{Pe}}\,. \tag{9}$$

Here T_e, Y_{Fe} and Y_{Pe} are values corresponding to chemical equilibrium given by the equations

$$T_e - T_u = \frac{q}{c_p}(Y_F - Y_{Fe}) = \frac{q}{c_p}Y_{Pe}$$

$$\rho Y_{Fe} B e^{-E/RT_e} - \rho Y_{Pe} B' e^{-E'/RT_e} = 0\,.$$

These values correspond to the equilibrium in the burnt gas behind an adiabatic unstrained planar premixed flame, for which the propagation speed (the laminar flame speed) is

$$S_L = \left[\frac{2\left[\mathrm{Le_F} + re^{-\alpha\psi}(\mathrm{Le_P} + \alpha^2\psi)\right]}{\beta^2} D_T B e^{-E/RT_e}\right]^{1/2},$$

where $\alpha \equiv (T_e - T_u)/T_e$, $\psi \equiv (E' - E)/R(T_e - T_u)$ and $r \equiv B'/B$. This expression can be derived in the asymptotic limit $\beta \gg 1$ as shown in [13]. We note that S_L reduces to the well-known expression of the laminar flame speed in the irreversible case when $r = 0$.

In obtaining the non-dimensional Equations (4)–(6), we have taken as unit length the mixing layer thickness $L \equiv \sqrt{2D_T/a}$ and $y = Y/L$. The parameters κ and ϵ, defined by $\kappa \equiv \beta(D_T/S_L^2)\hat{\kappa}$ and $\epsilon \equiv D_T/LS_L = \sqrt{D_T a}/S_L\sqrt{2}$, represent a non-dimensional measure of the heat-loss intensity and strain, respectively. Finally, the non-dimensional reaction rate

is given by

$$\omega \equiv \frac{\beta^2}{2\left[\mathrm{Le_F} + re^{-\alpha\psi}(\mathrm{Le_P} + \alpha^2\psi)\right]}\,\phi\,\exp\left(\frac{\beta(\theta-1)}{1+\alpha(\theta-1)}\right), \tag{10}$$

where

$$\phi = y_F + re^{-\alpha\psi} - ry_P \exp\left(\frac{-\alpha\psi}{1+\alpha(\theta-1)}\right). \tag{11}$$

We note that when the reversibility parameter r is zero, we recover the reaction rate of the irreversible case. We also point out that the presence of three terms in ϕ is due to our choice of the scaled mass fractions given in Equation (9).

At this stage the formulation of the problem is complete and is given by Equations (4)–(6) with boundary conditions (7)–(8). The main parameters relevant to this study are ϵ, κ, r, in addition to β, $\mathrm{Le_F}$ and $\mathrm{Le_P}$. The paper is devoted to an asymptotic analysis of the problem in the limit $\beta \to \infty$, which is presented in the next section.

3. Asymptotic analysis

3.1. *Preliminaries*

In the limit $\beta \to \infty$, we postulate that the chemical term is dominant in an infinitely thin reaction layer, located at $y = y_*$, say. The reaction layer separates the unburnt gas region, where the reaction term is exponentially small, as in the irreversible case, from the burnt gas region where quasi-equilibrium prevails. We say, *quasi*-equilibrium because, as we shall confirm, the reaction term is typically $\mathcal{O}(\beta^{-1})$, whenever the reversibility parameter r is non-zero.[1] This is in marked contrast with the irreversible case, where the reaction term is zero to all orders in β^{-1} in the burnt gas. This difficulty can be elegantly circumvented, however, as we now demonstrate. To this end, we assume that the Lewis numbers are close to unity, more precisely that

$$\mathrm{Le_F} \sim 1 + \frac{l_F}{\beta} \quad \text{and} \quad \mathrm{Le_P} \sim 1 + \frac{l_P}{\beta}, \tag{12}$$

where l_F and l_P are order $\mathcal{O}(1)$ constants. This assumption along with the fact that the heat-loss term is $\mathcal{O}(\beta^{-1})$ implies the leading order relations $y_F^0 + \theta^0 = 1$, $y_P^0 - \theta^0 = 0$, everywhere in the domain, and

$$\theta^0 = 1, \quad y_F^0 = 0, \quad y_P^0 = 1 \qquad \text{in the burnt gas} \quad 0 \le y \le y_*. \tag{13}$$

This is easily seen on introducing expansions[2] of the form

$$y_F = y_F^0 + \beta^{-1}y_F^1 + \cdots, \quad y_P = y_P^0 + \beta^{-1}y_P^1 + \cdots, \quad \theta = \theta^0 + \beta^{-1}\theta^1 + \cdots \tag{14}$$

into Equations (4)–(8), and noting that the governing equations for $y_F^0 + \theta^0$ and $y_P^0 - \theta^0$ are free from source terms.

Before proceeding with the analysis, we pause to highlight a key difference between the irreversible and reversible cases related to the equilibrium in the burnt gas mentioned above. In the former case, the reaction rate ω given by (10) with $\phi = y_F$ (on setting $r = 0$ in (11)), is transcendentally small, on account of $y_F = 0$ to all orders in β^{-1} in the burnt gas. Indeed, if $y_F \sim \gamma\beta^{-n}$ for some positive number n is substituted into (5), one obtains

$$-2y\frac{d\gamma}{dy} \sim \frac{1}{\mathrm{Le_F}}\frac{d^2\gamma}{dy^2} - \frac{\epsilon^{-2}\exp\theta^1}{2\mathrm{Le_F}}\beta^2\gamma\,,$$

implying that γ must be zero, since otherwise the last term cannot be balanced in the limit $\beta \to \infty$. A similar approach in the reversible case, using (10), (11), (13) and (14), leads to

$$-2y\frac{dy_F^1}{dy} \sim \frac{1}{\mathrm{Le_F}}\frac{d^2y_F^1}{dy^2} - \frac{\epsilon^{-2}\exp\theta^1}{2\left[\mathrm{Le_F} + re^{-\alpha\psi}(\mathrm{Le_P} + \alpha^2\psi)\right]}\beta^3\left(\phi^0 + \frac{\phi^1}{\beta} + \frac{\phi^2}{\beta^2} + \cdots\right),$$

in the burnt gas. This implies that $\phi^0 = 0$, $\phi^1 = 0$ and $\phi^2 = 0$, otherwise the reaction term cannot be balanced as $\beta \to \infty$, and

$$-2y\frac{dy_F^1}{dy} \sim \frac{1}{\mathrm{Le_F}}\frac{d^2y_F^1}{dy^2} - \frac{\epsilon^{-2}\exp\theta^1}{2\left[\mathrm{Le_F} + re^{-\alpha\psi}(\mathrm{Le_P} + \alpha^2\psi)\right]}\phi^3\,. \tag{15}$$

On using (11), the condition $\phi^0 = 0$ is trivially satisfied on account of (13), while the condition $\phi^1 = 0$ takes the form

$$y_F^1 - re^{-\alpha\psi}y_P^1 - re^{-\alpha\psi}\alpha^2\psi\theta^1 = 0\,. \tag{16}$$

At this stage, on inspecting (15) (and similar equations for θ^1 and y_P^1), we note that the $\mathcal{O}(\beta^{-1})$ problem is not closed in the burnt gas, due to the presence of ϕ^3 in the chemical source term (involving second and third orders of expansion). We note however, that this difficulty can be avoided if one works with the variables $h \equiv \theta^1 + y_F^1$ and $k \equiv \theta^1 - y_P^1$, which are governed by equations free from reaction terms.

3.2. *Reformulation and jump conditions*

More precisely, in terms of θ^0, h, and k, the problem consists in solving

$$-2y\frac{d\theta^0}{dy} = \frac{d^2\theta^0}{dy^2} \tag{17}$$

$$-2y\frac{dh}{dy} = \frac{d^2h}{dy^2} + l_F\frac{d^2\theta^0}{dy^2} - \epsilon^{-2}\kappa\,\theta^0 \tag{18}$$

$$-2y\frac{dk}{dy} = \frac{d^2k}{dy^2} + l_P\frac{d^2\theta^0}{dy^2} - \epsilon^{-2}\kappa\,\theta^0, \tag{19}$$

for $y \neq y_*$, subject to the boundary conditions

$$\theta^0 = 0, h = 0, k = 0 \quad \text{as } y \to \infty \tag{20}$$

$$\frac{dh}{dy} = \frac{dk}{dy} = 0 \quad \text{at } y = 0\,, \tag{21}$$

and appropriate jump conditions at $y = y_*$. The jump conditions can be derived using a methodology commonly used in the irreversible case (see e.g. [1, p. 39] and [17, p. 527]), and are found to be

$$\left[\theta^0\right] = [h] = [k] = 0 \tag{22}$$

$$\left[\frac{dh}{dy}\right] + l_F\left[\frac{d\theta^0}{dy}\right] = 0\,, \quad \left[\frac{dk}{dy}\right] + l_P\left[\frac{d\theta^0}{dy}\right] = 0 \tag{23}$$

$$\left[\frac{d\theta^0}{dy}\right] = \epsilon^{-1}\exp\left(\frac{h_* + re^{-\alpha\psi}k_*}{2\left\{1 + re^{-\alpha\psi}(1+\alpha^2\psi)\right\}}\right) \tag{24}$$

with the notation $[f] = f(y_*^-) - f(y_*^+)$, and where $h_* \equiv h(y_*^-)$ and $k_* \equiv k(y_*^-)$. In fact, (22) simply expresses the continuity of the profiles at y_*, while (23) can be obtained by integration of Equations (18) and (19) across the thin reaction layer located at $y = y_*$, these equations being valid everywhere. As for jump condition (24), it can be derived as follows. We introduce a stretched variable η and inner expansions in the thin reaction layer given by

$$y = y_* + \frac{\eta}{\beta}, \quad \theta \sim 1 + \frac{\Theta^1(\eta)}{\beta}, \quad y_F \sim \frac{F^1(\eta)}{\beta}, \quad y_P \sim 1 + \frac{P^1(\eta)}{\beta}\,. \tag{25}$$

To leading order, the governing equations (4)–(6) then imply that

$$\frac{d^2\Theta^1}{d\eta^2} + \frac{\epsilon^{-2}}{2}\left\{\frac{F^1 - re^{-\alpha\psi}(P^1 + \alpha^2\psi\Theta^1)}{1 + re^{-\alpha\psi}(1+\alpha^2\psi)}\right\}\exp\Theta^1 = 0$$

$$\frac{d^2(\Theta^1 + F^1)}{d\eta^2} = 0\,, \qquad \frac{d^2(\Theta^1 - P^1)}{d\eta^2} = 0\,.$$

The last two equations are readily integrated to yield $F^1 = h_* - \Theta^1$ and $P^1 = \Theta^1 - k_*$, after using the matching requirement with the outer solution in the burnt gas that $\Theta^1 = \theta^1(y_*^-)$, $F^1 = y_F^1(y_*^-)$ and $P^1 = y_P^1(y_*^-)$ as $\eta \to -\infty$. Eliminating F^1 and P^1, the inner problem reduces to

$$\frac{d^2\Theta^1}{d\eta^2} + \frac{\epsilon^{-2}}{2}(\bar{h}_* - \Theta^1)\exp\Theta^1 = 0\,, \tag{26}$$

where

$$\bar{h}_* \equiv \frac{h_* + re^{-\alpha\psi}k_*}{1 + re^{-\alpha\psi}(1+\alpha^2\psi)}\,. \tag{27}$$

We note that the quasi-equilibrium condition (16), along with the definitions of h and k, imply that $\bar{h}_*$ thus defined is the perturbation in the flame temperature, namely $\bar{h}_* = \theta^1(y_*^-)$. Now, we multiply Equation (26) by $d\Theta^1/d\eta$, then integrate with respect to η

using the matching conditions

$$\Theta^1 = \bar{h}_* \quad \text{as} \quad \eta \to -\infty \qquad \text{and} \qquad \Theta^1 = \bar{h}_* + \eta \frac{d\theta^0}{dy}(y_*^+) \quad \text{as} \quad \eta \to \infty \tag{28}$$

to obtain

$$\left(\frac{d\theta^0}{dy}\right)^2\Bigg|_{y=y_*^+} = \epsilon^{-2} \int_{\bar{h}_*}^{-\infty} (\Theta^1 - \bar{h}_*) \exp \Theta^1 \, d\Theta^1 = \epsilon^{-2} \exp \bar{h}_* \, .$$

Thus, $d\theta^0/dy(y_*^+) = -\epsilon^{-1} \exp(\bar{h}_*/2)$, which yields jump condition (24), given the definition of $\bar{h}_*$ in (27) and the fact that $d\theta^0/dy(y_*^-) = 0$ on account of (13).

3.3. *Reduction of the problem with reversible reaction to that with an irreversible reaction*

In the previous section, we have provided a reformulation of the problem in terms of θ^0, $h \equiv \theta^1 + y_F^1$, and $k \equiv \theta^1 - y_P^1$, given by Equations (17)–(24). In arriving at this reformulation, we emphasize the importance of the near-equidiffusion assumption (12) and the use of the quasi-equilibrium condition in the burnt gas (16) which has led to expression (27) for the perturbation in the flame temperature $\bar{h}_* \equiv \theta^1(y_*)$. In fact, a major simplification of the problem can be achieved by introducing an effective excess enthalpy $\bar{h}$, a linear combination of h and k suggested by (27) given by

$$\bar{h} \equiv \frac{h + re^{-\alpha\psi} k}{1 + re^{-\alpha\psi}(1 + \alpha^2 \psi)} \, . \tag{29}$$

This combination is seen, on using (16) and (29), to be such that $\bar{h} = \theta^1$, or,

$$\theta \sim 1 + \frac{\bar{h}}{\beta} \qquad \text{in the burnt gas} \quad 0 \le y \le y_* \, . \tag{30}$$

In terms of θ^0 and $\bar{h}$, Equations (17)–(24) imply that the problem can be written as

$$-2y \frac{d\theta^0}{dy} = \frac{d^2\theta^0}{dy^2} \tag{31}$$

$$-2y \frac{d\bar{h}}{dy} = \frac{d^2\bar{h}}{dy^2} + \bar{l} \frac{d^2\theta^0}{dy^2} - \epsilon^{-2} \bar{\kappa} \, \theta^0 \tag{32}$$

for $y \neq y_*$, subject to the boundary conditions

$$\theta^0 = 0, \bar{h} = 0 \quad \text{as } y \to \infty \tag{33}$$

$$\frac{d\bar{h}}{dy} = 0 \quad \text{at } y = 0 \, , \tag{34}$$

and the jump conditions

$$\left[\theta^0\right] = \left[\bar{h}\right] = 0 \tag{35}$$

$$\left[\frac{d\bar{h}}{dy}\right] + \bar{l}\left[\frac{d\theta^0}{dy}\right] = 0 \tag{36}$$

$$\left[\frac{d\theta^0}{dy}\right] = \epsilon^{-1}\exp\frac{\bar{h}}{2} \tag{37}$$

at $y = y_*$. Here, we have introduced the parameters

$$\bar{l} = \frac{l_F + l_P r e^{-\alpha\psi}}{1 + r e^{-\alpha\psi}(1+\alpha^2\psi)} \qquad \text{and} \qquad \bar{\kappa} = \frac{1 + r e^{-\alpha\psi}}{1 + r e^{-\alpha\psi}(1+\alpha^2\psi)}\kappa\,. \tag{38}$$

Thus, $\bar{l}$ and $\bar{\kappa}$ appear as an effective reduced Lewis number and an effective heat-loss coefficient, and simplify the analysis by significantly reducing the number of parameters.

More importantly, we note that the introduction of $\bar{h}$, $\bar{l}$, and $\bar{\kappa}$ formally reduces the problem with reversible reaction to a familiar problem with an irreversible reaction, for which, of course, $\bar{l} = l_F$, $\bar{\kappa} = \kappa$, and $\bar{h} = h$. The three additional non-dimensional parameters r, ψ and l_P introduced by the reversibility of the reaction can thus be simply accounted for by (38), without extra cost.

3.4. *The quasi-equilibrium in the burnt gas*

At this stage, and without the need to solve the equations, which we do in the next section, we can show that the reaction rate ω is precisely $\mathcal{O}(\beta^{-1})$ in the burnt gas, provided the reversibility parameter r and heat-loss coefficient κ are both non-zero. Indeed, in the burnt gas, Equation (4) implies that

$$\epsilon^{-2}\omega \sim \beta^{-1}\left(-2y\frac{d\bar{h}}{dy} - \frac{d^2\bar{h}}{dy^2} + \epsilon^{-2}\kappa\right),$$

when used with Equation (30), while Equation (32) reduces to

$$-2y\frac{d\bar{h}}{dy} = \frac{d^2\bar{h}}{dy^2} - \epsilon^{-2}\bar{\kappa}\,.$$

It follows that

$$\omega \sim \beta^{-1}(\kappa - \bar{\kappa})\,,$$

that is, using (38), that

$$\omega \sim \beta^{-1}\kappa r\,\frac{\alpha^2\psi e^{-\alpha\psi}}{1 + r e^{-\alpha\psi}(1+\alpha^2\psi)}\,, \tag{39}$$

justifying our claim that ω is precisely $\mathcal{O}(\beta^{-1})$ unless $\kappa r = 0$.

3.5. *Analytical solution*

We proceed now to solving the problem of Section (3.3). The results will be expressed in terms of the effective parameters $\bar{l}$ and $\bar{\kappa}$ given in (38), which incorporate reversibility.[3]

In the burnt gas region ($y < y_*$), we find

$$\theta^0 = 1$$
$$\bar{h} = \bar{h}_* - \frac{\bar{\kappa}\sqrt{\pi}}{2\epsilon^2}\left([\mathrm{erf}(y_*) - \mathrm{erf}(y)]\int_0^{y_*} e^{u^2}du + \int_{y_*}^{y}[\mathrm{erf}(u) - \mathrm{erf}(y)]\,e^{u^2}du\right).$$

In the unburnt gas region ($y > y_*$) we find

$$\theta^0 = \Gamma_1$$
$$h = \bar{h}_*\Gamma_1 + \bar{l}\Gamma_2 - \bar{\kappa}\Gamma_3\,,$$

where

$$\Gamma_1 = \frac{\mathrm{erfc}(y)}{\mathrm{erfc}(y_*)}, \qquad \Gamma_2 = \frac{ye^{-y^2}\mathrm{erfc}(y_*) - y_*e^{-y_*^2}\mathrm{erfc}(y)}{\sqrt{\pi}\,\mathrm{erfc}^2(y_*)},$$
$$\Gamma_3 = \frac{\sqrt{\pi}}{2\epsilon^2\mathrm{erfc}^2(y_*)}\left([\mathrm{erf}(y) - \mathrm{erf}(y_*)]\int_{y_*}^{\infty}\mathrm{erfc}^2(u)e^{u^2}du\right.$$
$$\left. -\mathrm{erfc}(y_*)\int_{y_*}^{y}[\mathrm{erf}(y) - \mathrm{erf}(u)]\,\mathrm{erfc}(u)e^{u^2}du\right).$$

Jump conditions (36) and (37) then yield

$$\bar{h}_* = \frac{-\bar{\kappa}\sqrt{\pi}}{2\epsilon^2\mathrm{erfc}(y_*)}a - \bar{l}b \tag{40}$$
$$\epsilon = \frac{\sqrt{\pi}}{2}\mathrm{erfc}(y_*)\exp\left(y_*^2 + \frac{\bar{h}_*}{2}\right), \tag{41}$$

where

$$a = \mathrm{erfc}^2(y_*)\int_0^{y_*}e^{u^2}du + \int_{y_*}^{\infty}\mathrm{erfc}^2(u)e^{u^2}du,$$
$$b = \frac{1}{2}\left[1 + 2y_*^2 - \frac{2y_*e^{-y_*^2}}{\sqrt{\pi}\,\mathrm{erfc}(y_*)}\right].$$

Equation (41) provides an expression for $\bar{h}_*$ as a function of ϵ and y_*, say $\bar{h}_* = \bar{h}_*(y_*;\epsilon)$, which when used in (40) yields an expression for $\bar{\kappa}$ in terms of y_*, ϵ and $\bar{l}$ of the form $\bar{\kappa} = \bar{\kappa}(y_*;\epsilon,\bar{l})$. That is, we have the two equations

$$\bar{h}_* = 2\ln\left(\frac{2\epsilon e^{-y_*^2}}{\sqrt{\pi}\,\mathrm{erfc}(y_*)}\right) \tag{42}$$

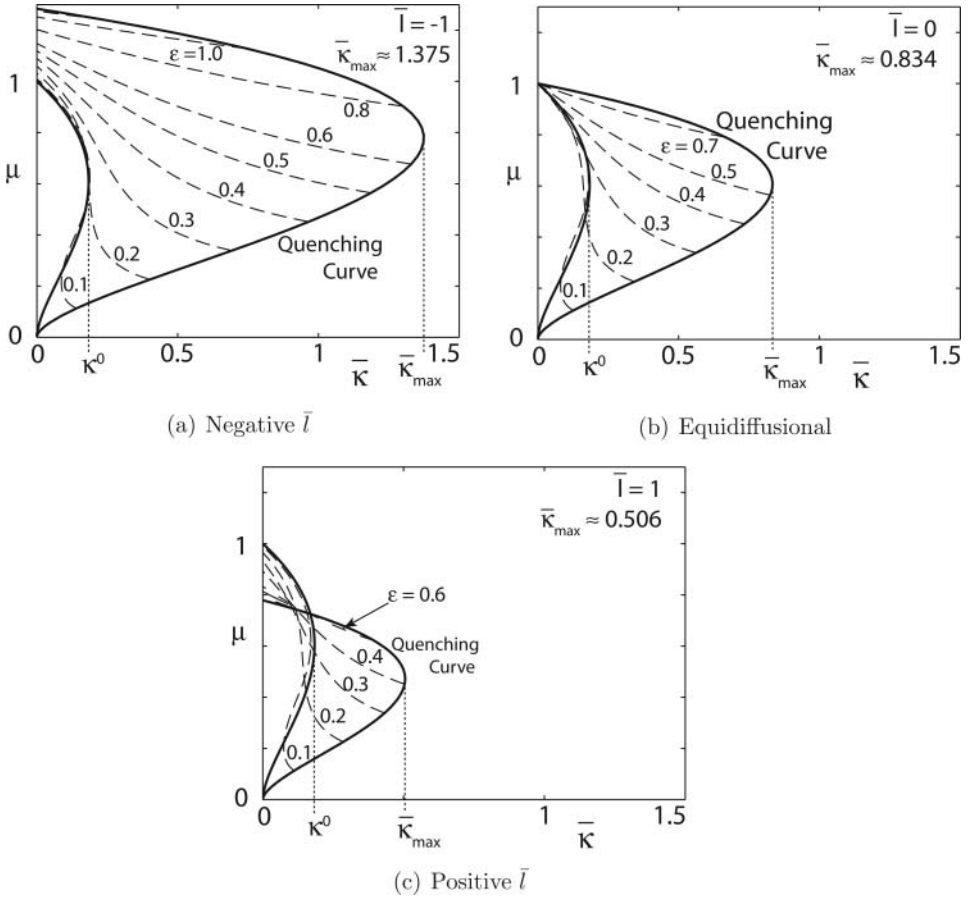

(a) Negative $\bar{l}$ (b) Equidiffusional

(c) Positive $\bar{l}$

Figure 2. The burning rate per unit flame area, μ, versus $\bar{\kappa}$ for selected values of ϵ, and three values of $\bar{l}$.

$$\bar{\kappa} = -\frac{2\epsilon^2 \mathrm{erfc}(y_*)}{a\sqrt{\pi}} \left(\bar{h}_* + \bar{l}b\right) . \tag{43}$$

For fixed values of ϵ and $\bar{l}$ and by varying y_*, Equations (42) and (43) provide a parametric plot of $\bar{h}_*$ (or the burning rate per unit flame area, $\mu \equiv \exp(\bar{h}_*/2)$), versus $\bar{\kappa}$. The results can be used, in particular, to delimit the domains of existence of the solutions in the $\bar{\kappa}$-ϵ plane.

4. Results and discussion

4.1. *Typical illustrative cases*

We begin with Figure 2, which shows plots of the burning rate per unit flame area, $\mu \equiv \exp(\bar{h}_*/2)$, versus $\bar{\kappa}$, for selected values of $\bar{l}$ and ϵ. The middle figure, Figure 2(b), is our reference case and corresponds to $\bar{l} = 0$. Figures 2(a) and 2(c) correspond to $\bar{l} = -1$ and $\bar{l} = 1$, respectively.

In each figure, the inner solid curve corresponds to $\bar{\kappa} = -\mu^2 \ln(\mu)$, which is the well-known relation between the burning rate of the non-adiabatic planar unstrained flame and the heat-loss coefficient; the turning point of this curve, at $\bar{\kappa} = \kappa^0 \equiv (2e)^{-1}$, corresponds to extinction and its lower branch is known to represent unstable solutions. Each dashed line corresponds to a fixed value of ϵ (or the strain rate), and depicts the dependence of μ on $\bar{\kappa}$. As can be seen, for vanishing strain, the dashed lines tend to the solid inner line, as one may expect given that in the limit as $\epsilon \to 0$, the burning rate of the flame must tend to that of a free deflagration. In each figure, it is observed that for ϵ smaller than a critical value ϵ_c (depending on $\bar{l}$), the μ versus $\bar{\kappa}$ curves are multivalued inverse S-shaped curves, exhibiting two turning points. The upper branches of the S-shaped curves consist of *strongly* burning solutions, and the lower branches, *weakly* burning solutions. The middle branches, however, are presumably unstable since they exhibit the unphysical behaviour of an increasing burning rate μ with $\bar{\kappa}$. For $\epsilon > \epsilon_c$, strongly burning solutions only are obtained. We note, in each figure, that all dashed curves terminate on the outer solid curve labelled 'quenching curve'. The quenching curve is the locus of the points corresponding to $y_* = 0$ which in view of Equations (42) and (43) is given by

$$\bar{\kappa} = -\frac{\epsilon^2}{c\sqrt{\pi}}\left[4\ln\left(\frac{2\epsilon}{\sqrt{\pi}}\right) + \bar{l}\right] \qquad \text{where} \quad c = \int_0^\infty \operatorname{erfc}^2(u) e^{u^2} du \approx 0.391\,, \tag{44}$$

or, since $\mu = 2\epsilon/\sqrt{\pi}$ when $y_* = 0$,

$$\bar{\kappa} = -\frac{\sqrt{\pi}\mu^2}{4c}\left[4\ln\mu + \bar{l}\right]. \tag{45}$$

This expression yields a maximum value of $\bar{\kappa}$ for $\mu = \exp(-\frac{1}{2} - \frac{\bar{l}}{4})$, which is given by

$$\bar{\kappa}_{\max} = \frac{\sqrt{\pi}}{2c}\exp\left(-1 - \frac{\bar{l}}{2}\right) \approx 2.27\exp\left(-1 - \frac{\bar{l}}{2}\right). \tag{46}$$

Comparing the figures, it is apparent that the range of $\bar{\kappa}$ for which burning solutions exist is reduced as $\bar{l}$ is increased. This observation is readily explained by Equation (46). For $\bar{l} = -1$, we find that $\bar{\kappa}_{\max} \approx 1.375$, a value which is nearly eight times greater than $\kappa^0 = (2e)^{-1} \approx 0.184$, the extinction value of the unstrained planar flame. For $\bar{l} = 1$, $\bar{\kappa}_{\max} \approx 0.506$, about three times greater than κ^0. Thus, in the presence of strain, burning solutions may be encountered for values of κ much larger than the planar flame extinction value κ^0. This is consistent with similar observations in studies of flammability limits using the counterflow configuration, see e.g. [1–5]. This fact ceases to be true, however, if $\bar{l}$ is above a critical value $\bar{l}_c$ (the value of $\bar{l}$ at which $\bar{\kappa}_{\max} = \kappa^0$), determined from Equation (46) to be

$$\bar{l}_c = \ln(\pi/c^2) \approx 3.04\,; \tag{47}$$

large Lewis number cases corresponding to $\bar{l} \geq \bar{l}_c$ will be considered in Section 4.3.

In fact a lot of information is contained in Figure 2 concerning the coupling between strain, heat-loss, and preferential diffusion. For example, it is seen that for sufficiently small values of κ, there is always a strongly burning solution which increases with increasing (moderate) strain rate ϵ for $\bar{l} < 0$, and decreases for $\bar{l} > 0$. For sufficiently high values of

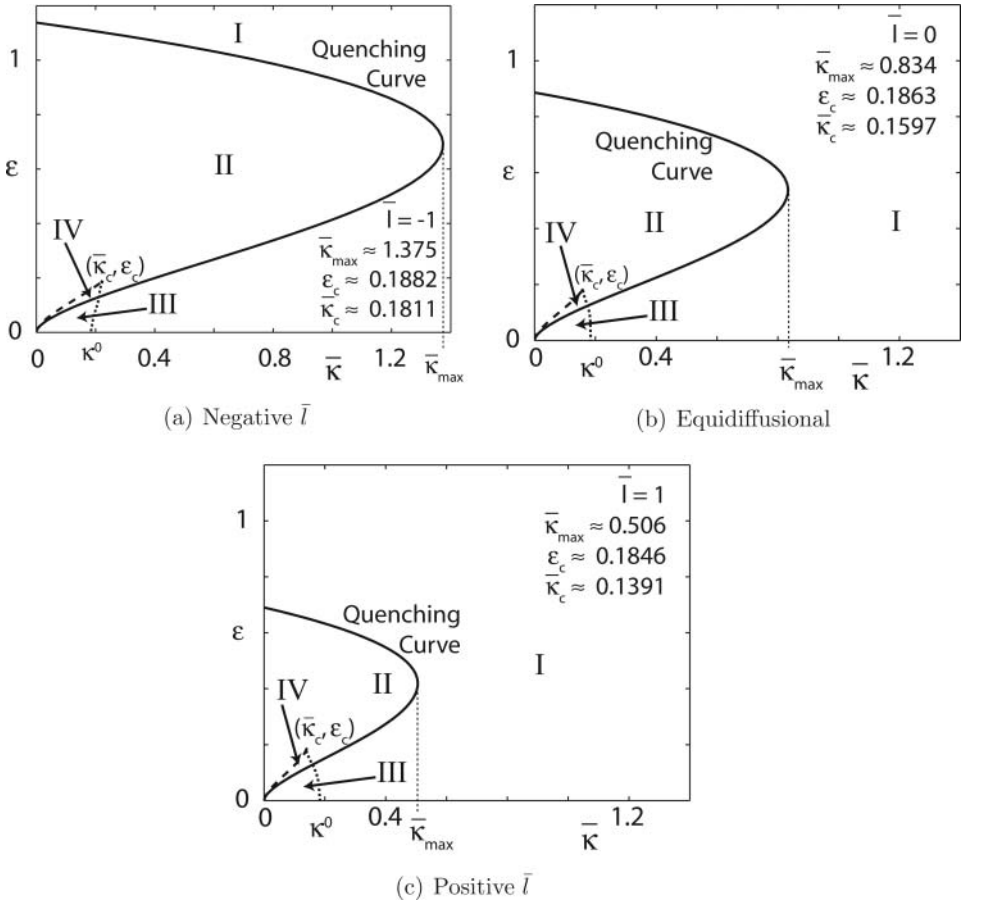

(a) Negative $\bar{l}$ (b) Equidiffusional

(c) Positive $\bar{l}$

Figure 3. The regions of solutions in the $\bar{\kappa}$-ϵ plane for three values of $\bar{l}$. The regions labelled I, II, III, and IV contain one, two, three, and four solutions, respectively, including the frozen solution.

$\bar{\kappa}$, however, μ is always an increasing function of ϵ, irrespective of $\bar{l}$. It is worth noting that the coupling between $\bar{\kappa}$, $\bar{l}$ and ϵ (or equivalent parameters) poses non-trivial difficulties, when interpreting flammability limit results as in [1–5], or in edge-flame studies [9]. The difficulties appear to be associated with the fact that, although the multiple solutions described above are fairly well known, they do not seem to have been fully located and classified in parameter spaces, at least as far as analytical studies are concerned. Therefore, it is useful to provide below bifurcation diagrams in the $\bar{\kappa}$-ϵ plane based on our analytical model for fixed values of $\bar{l}$.

4.2. *Bifurcation diagrams in the $\bar{\kappa}$-ϵ plane*

Figure 3 represents diagrams in the two-dimensional $\bar{\kappa}$-ϵ plane where regions characterizing the multiplicity of the solutions are delimited. The diagrams correspond to the same values of $\bar{l}$ as in Figure 2, namely $\bar{l} = -1$, 0 and 1 from top to bottom.

In each subfigure, the solid curve is the quenching curve, obtained from Equation (44). It can be seen from this curve that for fixed $\bar{\kappa} < \bar{\kappa}_{\max}$, there exist two quenching points, one for (moderately) large values of ϵ which is often termed the quenching limit in flammability

studies, since this type of extinction point exists even in the adiabatic case, and one for small values of ϵ, which is called the radiation limit, see e.g. [1–3]. The dotted line represents the upper turning points, say E, in the inverse S-shaped curves described above and the dashed line represents the locus of their lower turning points, say I. Typically, the point E corresponds to an extinction event (a jump from a strongly burning solution to a frozen solution, $\mu = 0$, as κ is increased), and the point I to a jump from a weakly burning (but not frozen) solution to a strongly burning one, as κ is decreased. The dashed and dotted lines meet, forming a cusp, at $(\bar{\kappa}_c, \epsilon_c)$. Of course ϵ_c is the critical value already introduced in discussing Figure 2, below which μ versus $\bar{\kappa}$ is a multivalued function. In fact, $(\bar{\kappa}_c, \epsilon_c)$ can be determined using Equation (43) and $d\bar{\kappa}/d\mu = d^2\bar{\kappa}/d\mu^2 = 0$, where derivatives are taken with ϵ kept fixed. The dashed and dotted lines themselves are determined from Equation (43) and the relation $d\bar{\kappa}/d\mu = 0$ which takes the form

$$\epsilon = \frac{A+1}{2y_*} \exp\left\{\frac{\bar{l}(aA+bB) - 2aA}{2(a-B)}\right\}$$

with $A = \sqrt{\pi}\, y_* e^{y_*^2} \mathrm{erfc}(y_*) - 1$ and $B = 2\mathrm{erfc}^2(y_*) \int_0^{y_*} e^{u^2} du$.

In each diagram, four regions are seen to be delimited by the quenching curve and the dashed and dotted lines. These regions are labelled I, II, III, and IV and contain one, two, three, and four solutions, respectively, including the frozen solution, $\mu = 0$. In region I, which lies outside the quenching curve and to the right of the dotted line, only the frozen solution exists. In region II, which lies inside the quenching curve and outside the cusp region, we have two solutions, a strongly burning solution and the frozen solutions. In region III, which lies below the quenching curve and to the left of the dotted line, we have three solutions, the frozen solution and two burning solutions, the lower of which is expected to be unstable (this belongs to the middle-branch of the inverse S-shaped curves in Figure 2). In region IV, which lies inside the cusp and above the quenching curve, we have four solutions, a strongly burning, a weakly burning, an intermediate (unstable), and a frozen solution.

The diagrams of Figure 3 show the overall dependence of the solutions of the non-adiabatic strained twin flame problem on the effective reduced Lewis number $\bar{l}$. All regions containing burning solutions (i.e. regions II, III, and IV) decrease in size in the parameter space $\bar{\kappa}$-ϵ as $\bar{l}$ is increased; simultaneously the peak of the cusp $(\bar{\kappa}_c, \epsilon_c)$ moves downwards and to the left, as does the tip of the quenching curve.

4.3. *Large Lewis number cases*

In this section, we briefly consider cases corresponding to values of the reduced Lewis number $\bar{l}$ larger than the critical value $\bar{l}_c \approx 3.04$ introduced in (47), for which $\bar{\kappa}_{\max} = \kappa^0$; here, as elsewhere in the text, $\bar{\kappa}_{\max}$ designates the maximum of $\bar{\kappa}$ on the quenching curve given by (46). For $\bar{l} \geq \bar{l}_c$, the maximum value of κ allowing burning planar solutions to exist, $\hat{\kappa}_{\max}$ say, is equal to the unstrained planar flame value κ^0 rather than $\bar{\kappa}_{\max}$ which is then smaller. In other words, we have

$$\hat{\kappa}_{\max} = \max\left[2.27 \exp\left(-1 - \frac{\bar{l}}{2}\right), \kappa^0\right], \tag{48}$$

an expression valid for all $\bar{l}$ which may be used to define a flammability limit.

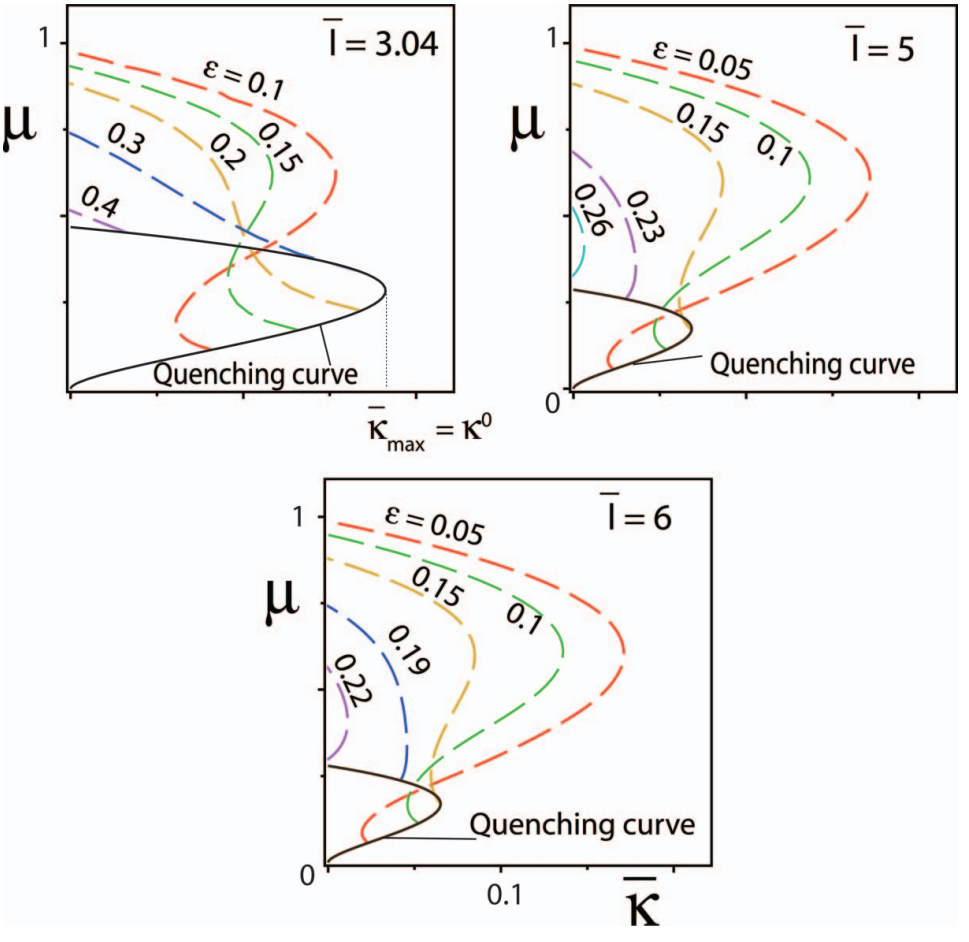

Figure 4. The burning rate per unit flame area, μ, versus $\bar{\kappa}$ for selected values of ϵ, and three values of $\bar{l}$.

Figure 4 shows the dependence of the burning rate μ on $\bar{\kappa}$ and ϵ, for three selected values of $\bar{l}$, increasing from top to bottom. The top subfigure corresponding to $\bar{l} = \bar{l}_c$ shows a behaviour similar to that observed in Figure 2; namely μ versus κ is a multivalued inverse-S shaped curve for small ϵ, and a single-valued monotonically decreasing function for larger values. For larger values of $\bar{l}$, such as those in the middle and bottom subfigures, additional inverse-C shaped curves appear for intermediate values of ϵ. Thus, one may expect a qualitative change in the bifurcation diagram. This is confirmed in Figure 5 which is to be compared to Figure 3. The regions labelled I, II, III, and IV, contain one, two, three, and four solutions, respectively, including the frozen solution. We note that the diagram consists of four such regions in the top subfigure; this is found to be the case for $\bar{l} < 4.03$. For $4.03 < \bar{l} < 5.15$, an additional region with three solutions, including the frozen solution, exists. This region is labelled III′ in the middle subfigure, and does not appear to have been identified in the literature. For $\bar{l} > 5.15$, as in the lower subfigure, regions III and III′ merge; in this subfigure region IV, close to the lower part of the quenching curve, is too small to be observable.

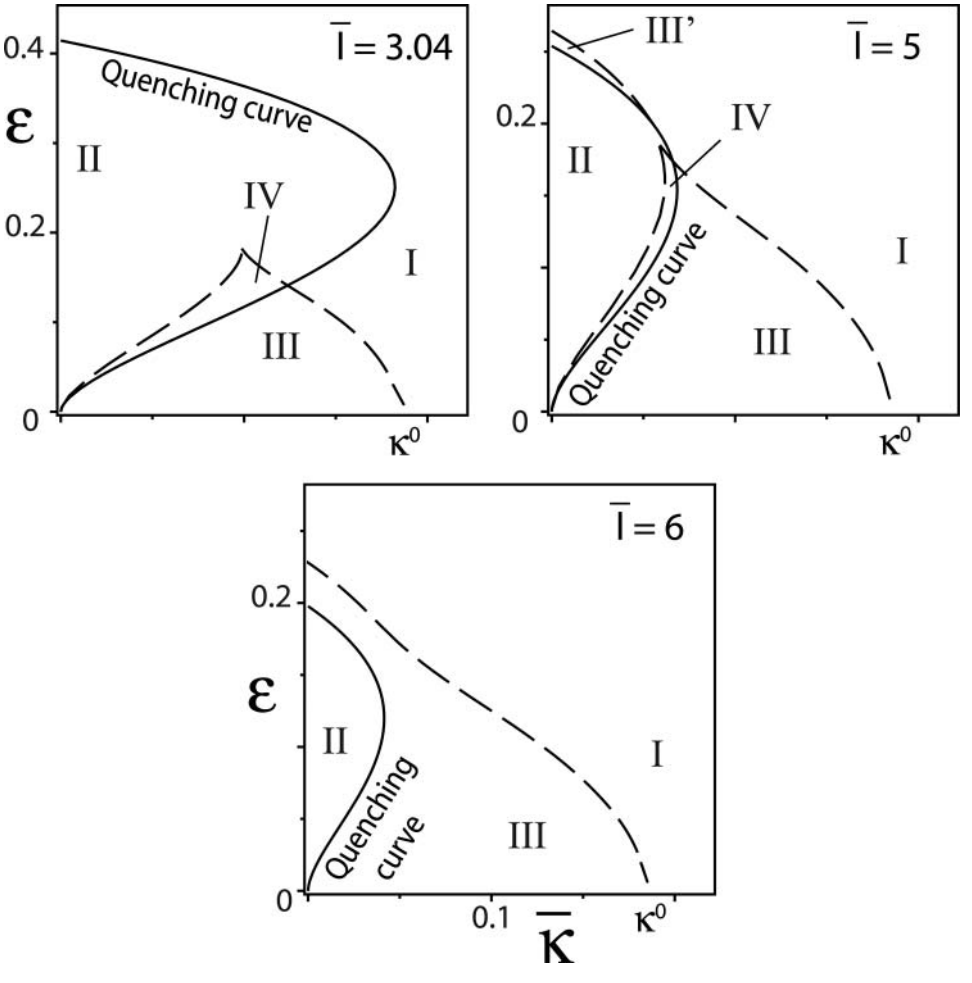

Figure 5. The regions of solutions in the $\bar{\kappa}$-ϵ plane for three values of $\bar{l}$. The regions labelled I, II, III, and IV contain one, two, three, and four solutions, respectively, including the frozen solution. The region labelled III′ contains three solutions, and exists for $4.03 < \bar{l} < 5.15$.

4.4. *Comparison with flammability limit studies and final remarks*

The results presented above are useful in the context of flammability limit studies, although not restricted to it. We have in mind more specifically studies carried out in the counterflow configuration, as in [1–5]. We refer the reader to these publications and the references therein for a detailed discussion. It should be emphasized here, however, that substantial difficulties in the interpretation of such results (experimental and numerical) seem to be associated with the crossing of the various regions of multiplicity of solutions as the physical parameters are varied. Our bifurcation diagrams presented in Figures 3 and 5 can be helpful in clarifying these difficulties. They are in fact consistent with those obtained numerically in [2, 4, 5], where equivalent diagrams have been constructed in a strain-rate versus equivalence-ratio plane.[4] Furthermore, fairly good agreement is found when comparing Figures 6, 8 and 9 of [2], carried out numerically within a one-step irreversible reaction, to our Figure 3, for example with respect to the dependence of the size of the burning regions and the location

of the cusp on the Lewis number. Similarly, Figure 9 of [4], and Figures 4, 5, 8, 11 and 16 of [5], obtained numerically within detailed chemistry models, are in good agreement[5] with our bifurcation diagrams 3 and 5. Our findings provide, however, additional analytical understanding, and convenient formulas such as 44 and 45 for the quenching curve, and 48 for the determination of $\hat{\kappa}_{\max}$, the maximum value of κ allowing burning planar solutions to exist. These complement the analytical results of [1], which does not contain a classification and bifurcation diagrams such as those of Figures 3 and 5.

Finally, we remind the reader that the effective parameters $\bar{l}$ and $\bar{\kappa}$ allow the reversibility of the reaction and the Lewis number of the product to be accounted for, if needed, by using the simple analytic expressions (38). For example, if $l_P = 0$, which is usually true in the case of combustion product(s) of typical mixtures such as hydrocarbons, it is seen from Equation (38) that an increase in the reversibility parameter r decreases the modulus of the effective Lewis number, whether positive or negative. Thus in a strongly reversible reaction, $\bar{l}$ is close to zero, i.e. preferential diffusion effects become negligible. In all cases reversibility decreases the effective heat-loss coefficient as prescribed by Equation (38). Other scenarios can be explained in a similar fashion.

5. Conclusions

We have conducted an analytical investigation of the twin planar flames in a counterflow configuration, accounting for non-adiabatic and non-equidiffusional conditions and the reversibility of the chemical reaction. The latter has been modelled by a single *reversible* reaction whose forward and backward rates are assumed to follow an Arrhenius law. The study has allowed for non-unit values of the Lewis numbers for both the (deficient) reactant and the product of combustion. Two main contributions have been made.

As a first contribution, we have identified fundamental differences in the asymptotic description of the flame between the reversible and irreversible cases, with the main difficulty identified being that the reaction rate ω is $\mathcal{O}(\beta^{-1})$, rather than exponentially small, in the burnt gas, when the reversibility parameter r and heat-loss coefficient κ are both non-zero. The difficulty has been overcome by a suitable generalization of the so-called near-equidiffusion flame approximation [18, p. 33] to the reversible case, including the derivation of appropriate jump conditions at the reaction sheet. As a result, we were able to reduce the analysis of the reversible case to that of the irreversible case by defining an effective reduced Lewis number and an effective heat-loss parameter $\bar{l}$ and $\bar{\kappa}$ given by (38). This demonstrates analytically, in this particular important configuration at least, that the results of the classical one-step irreversible chemistry model extend to one-step reversible chemistry.

As a second contribution, we have provided a full analytical treatment of planar non-adiabatic strained flames, complementing the results of [1]. In particular, convenient formulas such as 44 and 45 for the quenching curve, and 48 for the determination of $\hat{\kappa}_{\max}$, the maximum value of κ allowing burning planar solutions to exist, have been given. Furthermore, the existence and multiplicity of the solutions encountered has been systematically discussed by delimiting several regions in two-dimensional strain-rate versus effective heat-loss diagrams for selected values of the effective reduced Lewis number $\bar{l}$. For $\bar{l} < 4.03$, the diagram consists of four regions with one, two, three, and four solutions, respectively, including the frozen solution. For $4.03 < \bar{l} < 5.15$, an additional region with three solutions exists, which does not seem to have been identified in other studies. For larger values of $\bar{l}$, the two regions with three solutions merge, and the region with four solutions is of insignificant size. Our (bifurcation) diagrams were found to be in good agreement with, and

complementary to, numerically determined diagrams in flammability limit studies [2, 4, 5] based on one-step and detailed chemistry models. Finally, we note that our analytical study did not address the stability of the stationary solutions described, which will be the subject of a future investigation; numerical stability studies have, however, been conducted, e.g. in [4].

Notes

1. See Equation (39) below.
2. To avoid possible confusion, we note that superscripts on the variables y_F, y_P, θ or any function of these, such as ϕ in (11), indicates orders of expansion in terms of the small parameter β^{-1}.
3. The reader who is not interested in reversibility needs only set $\bar{l} = l_F$ and $\bar{\kappa} = \kappa$.
4. A decreasing equivalence ratio in these references corresponds to an increasing non-dimensional heat-loss $\bar{\kappa}$ in the present paper.
5. Compare in particular the large Lewis number case of Figure 16 of [5] to the bottom subfigure of Figure 5 of the present paper.

References

[1] J.D. Buckmaster, *The effects of radiation on stretched flames*, Combust. Theory Model. 1 (1997), pp. 1–11.
[2] Y. Ju, *Flame bifurcations and flammable regions of radiative counterflow premixed flames with general Lewis numbers*, Combust. Flame 113 (1998), pp. 603–614.
[3] H. Guo, Y. Ju, K. Maruta, T. Niioka, and F. Liu, *Radiation extinction limit of counterflow premixed lean methane–air flames*, Combust. Flame 109 (1997), pp. 639–646.
[4] Y. Ju and Y. Xue, *Extinction and flame bifurcations of stretched dimethyl ether premixed flames*, Proc. Combust. Inst. 30 (2005), pp. 295–301.
[5] Y. Ju, F. Liu, and H. Guo, *Effects of the Lewis number and radiative heat-loss on the bifurcation and extinction of* CH_4/O_2-N_2-He *flames*, J. Fluid Mechan. 379 (1999), pp. 165–190.
[6] J.B. Liu and P.D. Ronney, *Premixed edge-flames in spatially varying straining flows*, Combust. Sci. Technol. 144 (1999), pp. 21–46.
[7] J. Daou, M. Matalon, and A. Liñán, *Premixed edge flames under transverse enthalpy gradients*, Combust. Flame 121 (2000), pp. 107–121
[8] J. Daou and A. Liñán, *Ignition and extinction fronts in counterflowing premixed reactive gases*, Combust. Flame 118 (1999), pp. 479–488.
[9] R. Daou, J. Daou, and J. Dold, *Effect of heat-loss on flame-edges in a premixed counterflow*, Combust. Theory Model. 7 (2003), pp. 221–242.
[10] Ya.B. Zeldovich, H.I. Barrenblatt, V.B. Librovich, and G.M. Makhviladze, *The Mathematical Theory of Combustion and Explosions*, Consultants Bureau, New York, 1985.
[11] J.F. Clarke, *Reaction-broadening in a hydrogen–oxygen diffusion flame*, Proc. R. Soc. A 312 (1969), pp. 65–83.
[12] F. Fendell, *Combustion in initially unmixed reactants for one-step reversible chemical kinetics*, Astronautica Acta 13 (1967), pp. 183–191.
[13] J. Daou, *Premixed flames with a reversible reaction: propagation and stability*, Combust. Theory Model. 12 (2008), pp. 349–365.
[14] N. Peters, *Premixed burning in diffusion flames – the flame zone model of Libby and Economos*, Int. J. Heat Transf. 22 (1979), pp. 691–703.
[15] A. Bonnet, *Travelling-wave solutions to combustion models for a reversible reaction*, SIAM J. Math Anal. 27 (1996), pp. 1270–1285.
[16] A.P. Aludushin, B.J. Matkowsky, and V.A. Volpert, *Stoichiometric flames and their stability* Combust. Flame 101 (1995), pp. 15–25.
[17] G. Joulin and P. Vidal, *Hydrodynamics and Nonlinear Instabilities*, Cambridge University, Cambridge, 1998.
[18] J.D. Buckmaster and G.S.S. Ludford, *Lectures on Mathematical Combustion*, Society for Industrial and Applied Mathematics, Philadelphia, 1983.